The Astrophysical Journal Letters, 727:L31 (6pp), 2011 February 1 doi:10.1088/2041-8205/727/2/L31

HST WFC3/IR OBSERVATIONS OF ACTIVE GALACTIC NUCLEUS HOST GALAXIES AT $z \sim 2$: SUPERMASSIVE BLACK HOLES GROW IN DISK GALAXIES*

Kevin Schawinski[1,2,7], Ezequiel Treister[3,8], C. Megan Urry[1,2,4], Carolin N. Cardamone[5], Brooke Simmons[2,4], and Sukyoung K. Yi[6]

[1] Department of Physics, Yale University, New Haven, CT 06511, USA; kevin.schawinski@yale.edu
[2] Yale Center for Astronomy and Astrophysics, Yale University, P.O. Box 208121, New Haven, CT 06520, USA
[3] Institute for Astronomy, 2680 Woodlawn Drive, University of Hawaii, Honolulu, HI 96822, USA
[4] Department of Astronomy, Yale University, New Haven, CT 06511, USA
[5] Department of Physics, Massachusetts Institute of Technology, 77 Massachusetts Avenue, Cambridge, MA 02139, USA
[6] Department of Astronomy, Yonsei University, Seoul 120-749, Republic of Korea
Received 2010 November 2; accepted 2010 December 6; published 2011 January 6

ABSTRACT

We present the rest-frame optical morphologies of active galactic nucleus (AGN) host galaxies at $1.5 < z < 3$, using near-infrared imaging from the *Hubble Space Telescope* Wide Field Camera 3, the first such study of AGN host galaxies at these redshifts. The AGNs are X-ray-selected from the Chandra Deep Field South and have typical luminosities of 10^{42} erg s$^{-1} < L_X < 10^{44}$ erg s^{-1}. Accreting black holes in this luminosity and redshift range account for a substantial fraction of the total space density and black hole mass growth over cosmic time; they thus represent an important mode of black hole growth in the universe. We find that the majority (∼80%) of the host galaxies of these AGNs have low Sérsic indices indicative of disk-dominated light profiles, suggesting that secular processes govern a significant fraction of the cosmic growth of black holes. That is, many black holes in the present-day universe grew much of their mass in disk-dominated galaxies and not in early-type galaxies or major mergers. The properties of the AGN host galaxies are furthermore indistinguishable from their parent galaxy population and we find no strong evolution in either effective radii or morphological mix between $z \sim 2$ and $z \sim 0.05$.

Key words: galaxies: active – galaxies: high-redshift – galaxies: Seyfert

Online-only material: color figures

1. INTRODUCTION

Host galaxy morphology is a key parameter in the joint formation of galaxies and supermassive black holes via active black hole growth phases (Schawinski et al. 2010b). In the local universe, black hole growth is associated with very different evolutionary stages of galaxies: early-type host galaxies feature black hole accretion in a specific time window after a rapidly suppressed burst of star formation that was induced by a merger event (Schawinski et al. 2007, 2010a, 2010b; Wild et al. 2007; Constantin et al. 2008), while black hole growth in late-type galaxies, which dominates active galactic nucleus (AGN) host galaxy sample by number, occurs in massive, stable disk galaxies with no obvious recent perturbations to star formation (Schawinski et al. 2010b). That is, major mergers do not seem to make up a large part of the AGN host galaxy population at low redshift, although puzzlingly the fraction of AGNs exhibiting signs of recent or ongoing interactions increases at the highest luminosities in unbiased, hard X-ray-selected samples such as the *Swift* BAT sample (Schawinski et al. 2009; Koss et al. 2010). In any case, accretion at $z \sim 0$ represents a negligible fraction of cosmic black hole growth, most of which occurred at high redshift.

The properties of AGN host galaxies during the peak epoch of both star formation and black hole growth at $z \sim 2$ have until very recently remained virtually inaccessible. Ground-based imaging does not offer sufficient angular resolution to resolve the AGN host galaxies, while most *Hubble Space Telescope* (*HST*) imaging was in optical bands that translates to the rest-frame ultraviolet at $z \sim 2$. With the installation of the new Wide Field Camera 3 (WFC3) on the *HST*, we now have available ultra-deep, high-resolution near-infrared images of AGNs at $z \sim 2$ which allow us to study the *rest-frame optical* properties of their host galaxies in detail. The F160W (*H*-band) filter corresponds approximately to the *V* band at $z \sim 2$, with spatial resolution comparable to or better than Sloan Digital Sky imaging at $z \sim 0.05$.[9]

In this Letter, we present the rest-frame optical morphologies of moderate luminosity AGNs (10^{42} erg s$^{-1} < L_X < 10^{44}$ erg s^{-1}; corresponding to $-23 \lesssim M_V \lesssim -18$) during the peak epoch of growth at $z \sim 2$. AGNs with these luminosities represent a significant fraction of the cosmic black hole growth in terms of both number density and in X-ray light emitted (e.g., Ueda et al. 2003; Hasinger et al. 2005). Throughout this Letter, we assume a ΛCDM cosmology with $h_0 = 0.7$, $\Omega_m = 0.27$, and $\Omega_\Lambda = 0.73$, in agreement with the most recent cosmological observations (Hinshaw et al. 2009).

2. DATA

2.1. Sample Selection

We select AGNs using X-ray data from the deep 2 Ms Chandra Deep Field South observations (Luo et al. 2008) in the WFC3

* Based on observations made with the NASA/ESA *Hubble Space Telescope*, obtained from the data archive at the Space Telescope Institute. STScI is operated by the association of Universities for Research in Astronomy, Inc., under the NASA contract NAS 5-26555.
[7] Einstein Fellow.
[8] Chandra Fellow.
[9] For Sloan Digital Sky Survey, the 1.″4 median seeing at $z = 0.05$ corresponds to 1.36 kpc, while for *HST* WFC3/IR, the 0.″13 (undersampled) pixel scale at $z = 2$ corresponds to 1.09 kpc.

Table 1
X-ray-selected AGN Host Galaxies in the WFC3/IR ERS Field

ID[a]	R.A. (J2000)	Decl. (J2000)	Redshift	Type[b]	$\log_{10}(L_{\rm X,obs})$ (erg s^{-1})	$\log_{10}(M_{\rm stellar})$[c] ($M_\odot$)	Eddington Ratio[d]	$M_{\rm V}$ AB mag
49190	03 32 19.9	−27 45 17.9	2.424	phot	44.05	10.24	0.84	−22.17
50057	03 32 06.7	−27 44 55.1	2.296	phot	42.94	10.25	0.06	−22.05
50333	03 32 03.0	−27 44 50.0	2.573	spec	44.06	10.39	0.57	−22.79
50634	03 32 04.0	−27 44 41.5	3.618	phot	43.52	10.23	0.25	−22.85
52141	03 32 10.9	−27 44 14.9	1.613	spec	44.35	10.08	2.60	−22.97
52399	03 32 14.8	−27 44 02.6	1.527	phot	42.78	10.32	0.04	−19.95
53849	03 32 15.1	−27 43 35.3	1.691	phot	43.02	10.81	0.02	−23.16
54369	03 32 01.6	−27 43 27.0	2.720	spec	44.47	10.41	1.38	−22.23
55062	03 32 25.7	−27 43 05.7	2.291	spec	44.39	10.89	0.30	−22.85
55620	03 32 24.2	−27 42 57.7	2.303	spec	43.39	10.54	0.08	−22.57
56112	03 32 20.0	−27 42 43.6	2.733	phot	43.86	10.07	0.87	−21.35
56769	03 32 20.2	−27 42 27.2	2.773	phot	43.58	...	...	−21.06
56954	03 32 14.1	−27 42 30.1	2.026	spec	42.99	10.49	0.04	−22.07
57420	03 32 25.2	−27 42 18.8	1.617	spec	44.00	11.05	0.08	−23.72
57805	03 32 15.0	−27 42 25.0	1.895	phot	43.80	11.48	0.02	−25.13
57859	03 32 15.8	−27 42 07.6	2.779	phot	43.32	10.71	0.04	−22.94
58039	03 32 33.9	−27 42 04.1	1.936	phot	42.85	10.85	0.01	−23.57
58224	03 32 15.2	−27 41 58.6	2.402	spec	43.47	10.56	0.09	−22.67
58330	03 32 05.0	−27 42 02.7	2.062	phot	43.16	10.40	0.07	−23.29
58509	03 32 12.7	−27 41 49.0	1.490	phot	43.02	9.91	0.19	−20.23
58657	03 32 08.3	−27 41 53.5	2.470	spec	43.68	10.35	0.26	−21.68
59060	03 32 17.1	−27 41 37.0	2.193	phot	43.85	10.57	0.21	−21.79
63732	03 32 35.4	−27 40 02.7	1.490	phot	42.60	10.27	0.03	−22.13

Notes.
[a] Catalog ID, see Cardamone et al. (2010b).
[b] Type of redshift: phot, photometric redshift; spec, spectroscopic redshift; see Cardamone et al. (2010b).
[c] Stellar mass as computed by Cardamone et al. (2010a).
[d] Black hole mass is calculated from this stellar mass following the relation of Häring & Rix (2004). Eddington ratios assume an X-ray to bolometric correction factor of 20. Since a substantial fraction of the total stellar mass is likely in a disk, the black hole masses are overestimates, which means that the Eddington ratios are lower limits.

Early Release Science (ERS) field covered by the near-infrared mosaic (Windhorst et al. 2010). The X-ray emission is a signpost for the presence of an accreting black hole. The K correction shifts the hard X-rays, where obscuration becomes unimportant, to the observed *Chandra* band, making X-ray selection highly efficient except for the most highly obscured, Compton-thick systems (e.g., Treister et al. 2009b). The flux limit of the 2 Ms *Chandra* data at $z \sim 2$ means that all our X-ray sources are more luminous than $L_{\rm X} \sim 10^{42}$ erg s^{-1} and thus are unlikely to be affected significantly by X-ray emission from star formation.

We identify the matched counterparts of the X-ray sources using the MUSYC catalog of Cardamone et al. (2010b), which includes either spectroscopic redshifts where available or highly accurate photometric redshifts derived from the combined broadband and medium-band photometry (Cardamone et al. 2010b; photo-z quality $q_z < 3$). A total of 23 X-ray AGNs, with WFC3/IR coverage and $z > 1.45$, constitute the sample investigated in this Letter. We list the basic properties of the X-ray-selected AGN host galaxies in Table 1 and show a selection of H-band cutouts in Figure 1. The mean and median redshifts of this sample are 2.21 and 2.29, respectively, with a standard deviation of 0.52. The highest redshift is 3.62. The mean and median observed X-ray luminosities are $10^{43.1}$ and $10^{43.3}$ erg s^{-1}, respectively, with a standard deviation of 1.41 dex.

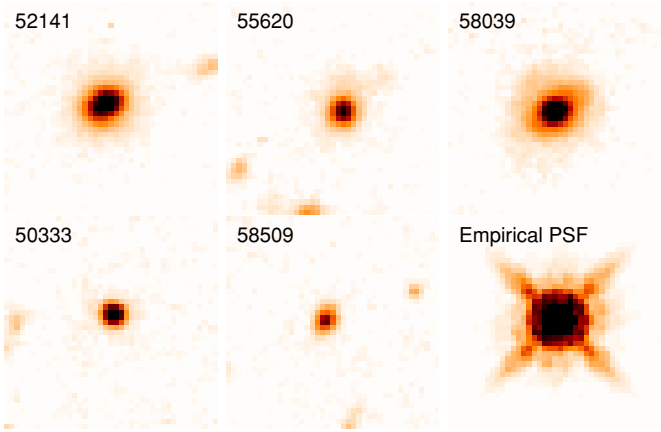

Figure 1. Sample H-band (F160W) cutouts measuring 5.″6 × 5.″6 of the X-ray-selected AGN host galaxies in our sample. In the top left of each cutout, we give the corresponding ID number (see Table 1). In the top row are galaxy-dominated AGN host galaxies while the left and middle of the bottom row are AGN-dominated sources. In the bottom-right panel, we show the empirical PSF generated from stars in the field.
(A color version of this figure is available in the online journal.)

2.2. WFC3/IR Image Reduction

We retrieved the WFC3/IR H-band (F160W) images taken as part of the ERS program from the archive and processed them with the standard STSDAS `pyraf` task `multidrizzle` (Koekemoer et al. 2002) to create a mosaicked F160W image of the entire ERS field. Using `multidrizzle`, we also created a noise image from the inverse variance map for each pixel, which takes into account the noise sources in each exposure, including read-noise, dark current, and sky background, as well as Poisson

noise from the sources themselves and dependence on exposure time. We then created cutouts for each X-ray source from both the *H*-band science and noise images for further analysis.

3. ANALYSIS

3.1. Image Analysis with GALFIT

We used the two-dimensional fitting algorithm GALFIT (Peng et al. 2002) to quantitatively analyze the light distribution of all X-ray-selected AGN host galaxies. We ran GALFIT on the *H*-band image cutout and associated noise map for each object. We manually masked all other sources in the cutout by setting the pixel values of the noise map to 10^9, thus giving them no weight in the fit. We built an empirical point-spread function (PSF) from a set of bright stars in the ERS field (see Figure 1, bottom right). Each star included in the empirical PSF was visually inspected for any possible contaminants from nearby stars. We checked that no star was under- or overexposed and that the final composite PSF fits well the individual stars regardless of their spectral energy distribution.

For each object, we fit three different models of the brightness distribution: (1) PSF-only fit, to determine whether the source is resolved; (2) Sérsic-only fit (Sersic 1968), to measure the Sérsic[10] n and the effective radius $r_{\rm eff}$; and (3) Sérsic + PSF fit, to represent an unobscured AGN point source.

The analysis of the two-dimensional light distribution of AGN host galaxies at high redshift poses two major challenges: the host galaxy may not be resolved and the host galaxy can be affected by the presence of a nuclear point source. First we determine which AGN host galaxies are resolved: following Bond et al. (2009) we compared the reduced χ^2 of the Sérsic and PSF fits to determine whether the Sérsic fit is significantly better than the PSF fit, i.e., there is some extra light that can be better fit if we allow for an extended source. That is, we determine

$$F = \frac{\left(\chi^2_{\rm PSF} - \chi^2_{\rm Sersic}\right)}{\chi^2_{\rm Sersic}} > F_{\rm crit}, \quad (1)$$

where $F_{\rm crit}$ is the critical value at which the Sérsic fit is significantly better. As Bond et al. (2009) argue, the value of $F_{\rm crit}$ cannot be determined from the F-distribution due to the behavior of GALFIT near minima and so $F_{\rm crit}$ should be determine empirically.

We therefore performed both Sérsic and PSF fits on a set of 18 faint ($R > 23$ AB) stars in the ERS field and calculated F for each. The values of F for these stars ranges from $F \sim -1$, where the Sérsic fit converges to an unphysically small radius and high n, to cases where F approaches ~0. The highest value we find is $F = -0.001$; to be safe, we adopt $F_{\rm crit} = 0.01$ as Bond et al. (2009) suggest.

This test removes 2 out of 23 AGN host galaxies. We also remove one source (ID 56769) that is too faint in the F160W image (see Koekemoer et al. 2004 who first described it; it is a real source and not a spurious X-ray detection). One of the resolved sources, ID 58330, required two components to adequately fit, which we from now on refer to as components A and B. We are left with 20 resolved AGN host galaxies. We also performed the Sérsic-only fit to a set of comparison galaxies matched in both *R*-band luminosity and redshift. We show an example fit in Figure 2.

[10] A value of Sérsic index $n = 1$ corresponds to a disk and $n = 4$ to an elliptical.

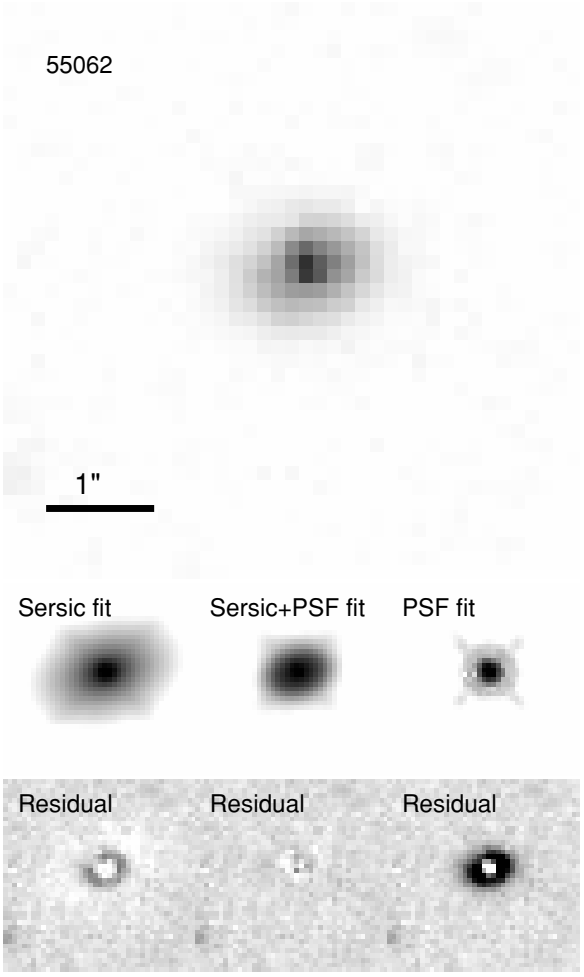

Figure 2. Example of an F160W images of AGN host galaxies and the GALFIT output for a galaxy dominated by starlight but containing a nuclear point source. Below the image are the three best-fit models (Sérsic-only, Sérsic + PSF, and PSF-only), with a logarithmic stretch, and below that are the corresponding residual images. The PSF-only residuals clearly show a resolved component that the PSF-only fit could not accommodate.

4. RESULTS

In Table 2, we report the results for all 20 AGN host galaxies[11] that are well resolved. For the final analysis, we needed to decide which fit to use. We therefore divide our sample into galaxy-dominated objects (lacking a strong nuclear point source) and AGN-dominated objects using the magnitude difference of the host galaxy to the AGN from the Sérsic + PSF fit. Specifically, we use the magnitude difference $\Delta m_{\rm AGN} = m_{\rm gal} - m_{\rm PSF} = -1$ as the partition (varying this does not significantly change the results). In what follows we quote the best Sérsic-only fit when the galaxy is at least 1 mag brighter than the point source, and the best Sérsic + PSF fit otherwise; we account for the two components of source ID 58330 separately. As discussed below, most fits favor low Sérsic indices, so for all fits with $n < 4$, we checked explicitly which fit better, a pure disk ($n = 1$, fixed) or a pure bulge ($n = 4$, fixed). In every case, the $n = 1$ fit has a lower χ^2 value. The systematics of decomposing nuclear point sources and extended host galaxies is discussed extensively by Simmons & Urry (2008) who show that as long as the point source is no more than four times brighter than the host galaxy,

[11] Twenty-one objects, if 58330A and B are counted individually.

Table 2
GALFIT Results for X-ray-selected AGN Host Galaxies at $z \sim 2$

ID[a]	Sérsic Fit Only			Sérsic + PSF Fit			$\Delta m_{\rm AGN}$
	Sérsic Index n	Angular $r_{\rm eff}$ ($''$)	Physical $R_{\rm eff}$ (kpc)	Sérsic Index n	Angular $r_{\rm eff}$ ($''$)	Physical $R_{\rm eff}$ (kpc)	(mag)
Galaxy-dominated, $\Delta m_{\rm AGN} = m_{\rm gal} - m_{\rm PSF} < -1$							
49190	0.52 ± 0.04	0.39 ± 0.05	3.15 ± 0.41	0.06 ± 0.09	0.46 ± 0.06	3.74 ± 0.49	-1.93
50057	10.44 ± 2.33	0.10 ± 0.01	0.78 ± 0.10	14.03 ± 5.09	0.07 ± 0.01	0.55 ± 0.07	-3.54
52141	1.65 ± 0.03	0.30 ± 0.04	2.53 ± 0.33	1.91 ± 0.04	0.31 ± 0.04	2.65 ± 0.34	-2.62
52399	1.29 ± 0.11	0.23 ± 0.03	1.99 ± 0.26	0.31 ± 0.10	0.34 ± 0.04	2.90 ± 0.38	-1.12
53849	3.52 ± 0.08	0.16 ± 0.02	1.32 ± 0.17	1.67 ± 0.08	0.23 ± 0.03	1.96 ± 0.25	-1.24
55062	0.89 ± 0.02	0.38 ± 0.05	3.08 ± 0.40	0.35 ± 0.02	0.44 ± 0.06	3.61 ± 0.47	-2.04
55620	2.37 ± 0.09	0.25 ± 0.03	2.03 ± 0.26	2.48 ± 0.09	0.27 ± 0.04	2.24 ± 0.29	-2.91
56112	1.99 ± 0.14	0.61 ± 0.08	4.79 ± 0.62	0.05 ± 0.04	0.77 ± 0.10	6.11 ± 0.79	-1.47
57805	8.33 ± 0.27	0.40 ± 0.05	3.39 ± 0.44	7.75 ± 0.23	0.35 ± 0.05	2.98 ± 0.39	-4.90
58039	6.35 ± 0.21	0.62 ± 0.08	5.22 ± 0.68	6.25 ± 0.21	0.58 ± 0.07	4.87 ± 0.63	-5.18
58330A	0.79 ± 0.05	0.31 ± 0.04	2.61 ± 0.34	0.74 ± 0.04	0.45 ± 0.06	3.76 ± 0.49	-1.51
58330B	2.28 ± 0.17	0.48 ± 0.06	4.04 ± 0.53	2.50 ± 0.18	0.44 ± 0.06	3.65 ± 0.47	-4.42
59060	0.55 ± 0.24	0.29 ± 0.04	2.37 ± 0.31	0.70 ± 0.07	0.26 ± 0.03	2.12 ± 0.28	-3.46
AGN-dominated, $\Delta m_{\rm AGN} = m_{\rm gal} - m_{\rm PSF} > -1$ (Sérsic-only fit may be unphysical))							
50333	3.66 ± 0.59	0.04 ± 0.01	0.28 ± 0.04	0.84 ± 0.49	0.15 ± 0.02	1.22 ± 0.16	0.95
56954	9.74 ± 1.96	1.60 ± 0.21	13.34 ± 1.73	0.17 ± 0.03	0.58 ± 0.08	4.87 ± 0.63	-0.89
57420	20.00 ± 8.11[b]	4.71 ± 0.61	39.87 ± 5.18	7.52 ± 0.47	0.36 ± 0.05	3.06 ± 0.40	-0.92
57859	1.62 ± 0.14	0.34 ± 0.04	2.63 ± 0.34	1.08 ± 0.17	0.39 ± 0.05	3.04 ± 0.40	0.73
58224	4.22 ± 0.40	0.11 ± 0.01	0.91 ± 0.12	0.97 ± 0.16	0.27 ± 0.04	2.17 ± 0.28	-0.19
58509	1.57 ± 0.18	0.14 ± 0.02	1.22 ± 0.16	0.06 ± 0.39	0.30 ± 0.04	2.57 ± 0.33	-0.23
58657	6.38 ± 3.16	0.03 ± 0.00	0.24 ± 0.03	0.05 ± 0.36	0.45 ± 0.06	3.65 ± 0.47	1.44
63732	20.00 ± 4.33[b]	7.68 ± 1.00	64.95 ± 8.44	0.97 ± 0.05	1.00 ± 0.13	8.43 ± 1.09	-0.55

Notes.
[a] Catalog ID, see Cardamone et al. (2010).
[b] The maximum value of the Sérsic index allowed is $n = 20$, so fits with $n = 20$ did not reach an acceptable minimum.

the fitted host galaxy parameters are reliable. In our sample, only one source comes close to this limit.

4.1. AGN Host Galaxies at $z \sim 2$

We show the distribution of Sérsic indices in Figure 3(a). The distribution is bimodal, with four AGN host galaxies having high Sérsic indices of $n > 4$ while the remaining population has low Sérsic indices. The mean and median Sérsic indices are $n = 2.54$ and $n = 1.08$, respectively. Most $z \sim 2$ AGN host galaxies ($16/20 \sim 80\%$) thus have disk-like light profiles while only a minority appear to be dominated by bulges. (Note that simulations show that at high redshift, disks and bulges can be confused, but for $n < 3$, at least half of the light is likely from the disk (Simmons & Urry 2008).) The distribution of disk versus spheroid morphology is qualitatively similar to that of the local AGN host galaxy population of ~10% early-type and ~90% late-types and indeterminate-type (i.e., Sa/S0) galaxies (Schawinski et al. 2010b).

We show the distribution of effective radii in Figure 3(b). The distribution is unimodal and the mean and median effective radii are 3.16 kpc and 3.04 kpc, respectively. We compare these effective radii to the AGN host galaxy sample at $z \sim 0.05$ presented by Schawinski et al. (2010b): the mean and median effective g-band[12] radii of this sample are 3.17 and 2.84 kpc, respectively, very similar to the high-redshift AGNs.

Figure 3 shows the histograms for the Sérsic indices, and effective radii of the matched comparison sample in Figure 3 and perform a Kolmogorov–Smirnov (K-S) test shows no evidence for the two populations being different; they are consistent with being drawn from the same parent distributions.

4.2. Black Hole Mass, Eddington Ratio, and Dark Matter Halo Mass

In order to give some context to the AGNs in our sample, we consider their black hole and dark matter halo masses. The majority of our objects are disk dominated so any black hole–stellar mass relation can only be taken as a general guide. From the stellar mass estimates described in Cardamone et al. (2010a) using the FAST algorithm (Kriek et al. 2009), we find that the AGN host galaxies in our sample have mean and median stellar masses of $10^{10}\,M_{\odot}$ and $2.5 \times 10^{10}\,M_{\odot}$, respectively. Using the black hole–bulge relation of Häring & Rix (2004), this should yield typical black hole masses of $5 \times 10^{7}\,M_{\odot}$. Given that this relation does not account for the mass of the disk which is included in our stellar mass estimate, this is an upper limit.

We calculate the Eddington ratios of our sources using the X-ray luminosity assuming an X-ray to bolometric correction of 20 and black hole masses, yielding mean and median Eddington ratios of 0.37 and 0.09, respectively (Table 1). Of course, the black hole masses are likely smaller (due to the contribution from the disk component), which means that the estimate for the Eddington ratio is a lower limit, and thus likely higher, which means that the objects in our sample are undergoing a period of significant mass growth. This is commensurate with the Eddington ratios of broad-line AGNs of comparable X-ray luminosity at this redshift of ~0.02–1 with the bulk at ~0.3 (Merloni et al. 2010; Trump et al. 2009).

[12] The g band is the closest band compared to the rest-frame wavelength of the $F160W$ H-band filter.

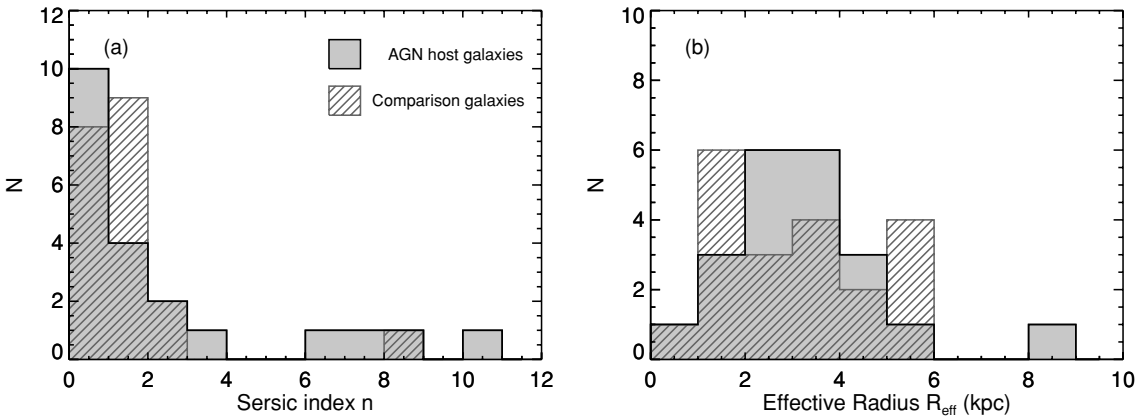

Figure 3. Morphologies and radii of AGN host and matched comparison galaxies. Left: the distribution of the of Sérsic indices n. Right: the physical effective radii $R_{\rm eff}$. The solid histogram represents the X-ray-selected AGN host galaxies at $z \sim 2$, while the striped histograms represent a matched comparison sample of normal galaxies. According to a Kolmogorov–Smirnov (K-S) test, the distributions of Sérsic indices and effective radii of the AGN host galaxies and inactive comparison galaxies are consistent with being drawn from the same parent distribution.

Finally, studies of the clustering of similar X-ray AGNs (e.g., Francke et al. 2008; Gilli et al. 2009) indicate that they reside in high-mass dark matter halos and that their $z = 0$ descendants are massive galaxies, most likely massive early-type galaxies with massive black holes. This means that these AGNs have grown into some of the most massive black holes locally.

5. DISCUSSION AND CONCLUSIONS

We have obtained the first clear view of the rest-frame optical morphologies of AGN host galaxies with Seyfert-like luminosities ($10^{42}\,{\rm erg\,s^{-1}} < L_{\rm X} < 10^{44}\,{\rm erg\,s^{-1}}$) at $z \sim 2$ using the new *HST* WFC3/IR in the ERS portion of the GOODS-S field. Fits to the host galaxy surface brightness profiles reveal that

1. The majority of these AGN host galaxies have low Sérsic indices, implying that the bulk of the host galaxy light comes from a disk.
2. The host galaxy structural parameters (Sérsic index and effective radius) do not appear to be significantly different from a comparison sample of inactive galaxies matched in redshift and luminosity.
3. The distribution of Sérsic indices implies that high-redshift AGN host galaxies have very similar morphologies to local AGN host galaxies, i.e., few early types but many late types. The typical effective radii are also similar to those of local AGN host galaxies.

These AGN host galaxies are a significant fraction of the total AGN population by number density and in terms of light emitted by accretion (Ueda et al. 2003; Hasinger et al. 2005). Using the X-ray luminosity function of Ueda et al. (2003) and evolution, obscuration distribution, and bolometric correction as described by Treister et al. (2009a), we estimate that the black hole growth in this population in the $z = 1.5$–3 range spanned by our sample represents 10%–17% of the total black hole growth over cosmic history. Excluding the most massive black holes, which get most of their mass in quasar-luminosity events triggered by mergers (Treister et al. 2010), 23%–40% of black hole growth occurs in a secular mode driven by internal processes in the host galaxy. Since disks also dominate the AGN host galaxy population at $z \sim 0$ (Schawinski et al. 2010b), where quasar-mode growth is unimportant, an even larger fraction of *all* black hole growth over cosmic history appears to take place in disk galaxies.

The results presented here show that moderate luminosity AGN host galaxies at $z \sim 2$ and $z \sim 0$ are remarkably similar. The high fraction of AGN host galaxies with disk-like light profiles is difficult to reconcile with the expectation of black holes growing jointly with stellar bulges during special phases of their evolution such as major mergers envisioned in many simulations (e.g., Springel et al. 2005; Hopkins et al. 2005, 2008). The disk morphologies of the host galaxies point instead to secular processes (e.g., Kormendy & Kennicutt 2004) as most common growth mode. The fact that AGN host galaxies are indistinguishable from the $z \sim 2$ comparison sample in terms of their Sérsic indices and effective radii further supports the role of secular growth. This is very different from the high-luminosity (quasar) population at the same redshift, which does seem to be driven by major mergers (Treister et al. 2010). Thus in the high-redshift universe, there appear to be two distinctly different modes of black hole growth for high- and low-luminosity AGNs.

The fact that the majority of black hole growth in this population—and by extension a significant fraction of cosmic black hole growth—occurs in a galaxy substantial disk means that it is not associated with major mergers. This raises interesting questions regarding the origin and relevance of the relationship between galaxy and black hole mass (Gebhardt et al. 2000; Ferrarese & Merritt 2000; Peng 2007; Jahnke & Maccio 2010). This secular black hole growth must still be self-regulated in some way that preserves the correlation between black hole mass and bulge mass.

Support for the work of K.S. and E.T. was provided by NASA through Einstein/Chandra Postdoctoral Fellowship grant numbers PF9-00069 and PF8- 90055, respectively, issued by the Chandra X-ray Observatory Center, which is operated by the Smithsonian Astrophysical Observatory for and on behalf of NASA under contract NAS8-03060. C.M.U. and C.C. acknowledge support from NSF grants AST-0407295, AST-0449678, AST-0807570, and Yale University. S.K.Y. acknowledges the support by the National Research Foundation of Korea through the Doyak grant (No. 20090078756) and the SRC grant to the Center for Galaxy Evolution Research. K.S. is grateful for the hospitality of the Astronomy Department at Yonsei University, Korea and thanks Yun-Kyeong Sheen, Sang-Il Han, and Andrew Fruchter for technical help. This research has made use of NASA's Astrophysics Data System Bibliographic Services.

Facilities: HST (WFC3), *CXO* (ACIS)

REFERENCES

Bond, N. A., Gawiser, E., Gronwall, C., Ciardullo, R., Altmann, M., & Schawinski, K. 2009, ApJ, 705, 639
Cardamone, C. N., Urry, C. M., Schawinski, K., Treister, E., Brammer, G., & Gawiser, E. 2010a, ApJ, 721, L38
Cardamone, C. N., et al. 2010b, ApJS, 189, 270
Constantin, A., Hoyle, F., & Vogeley, M. S. 2008, ApJ, 673, 715
Ferrarese, L., & Merritt, D. 2000, ApJ, 539, L9
Francke, H., et al. 2008, ApJ, 673, L13
Gebhardt, K., et al. 2000, ApJ, 539, L13
Gilli, R., et al. 2009, A&A, 494, 33
Häring, N., & Rix, H.-W. 2004, ApJ, 604, L89
Hasinger, G., Miyaji, T., & Schmidt, M. 2005, A&A, 441, 417
Hinshaw, G., et al. 2009, ApJS, 180, 225
Hopkins, P. F., Hernquist, L., Cox, T. J., Di Matteo, T., Martini, P., Robertson, B., & Springel, V. 2005, ApJ, 630, 705
Hopkins, P. F., Hernquist, L., Cox, T. J., & Kereš, D. 2008, ApJS, 175, 356
Jahnke, K., & Maccio, A. 2010, arXiv:1006.0482
Koekemoer, A. M., Fruchter, A. S., Hook, R. N., & Hack, W. 2002, HST Calibration Workshop, ed. S. Arribas, A. Koekemoer, & B. Whitmore (Baltimore, MD: STScI), 337
Koekemoer, A. M., et al. 2004, ApJ, 600, L123
Kormendy, J., & Kennicutt, R. C., Jr. 2004, ARA&A, 42, 603
Koss, M., Mushotzky, R., Veilleux, S., & Winter, L. 2010, ApJ, 716, L125
Kriek, M., van Dokkum, P. G., Labbé, I., Franx, M., Illingworth, G. D., Marchesini, D., & Quadri, R. F. 2009, ApJ, 700, 221
Luo, B., et al. 2008, ApJS, 179, 19
Merloni, A., et al. 2010, ApJ, 708, 137
Peng, C. Y. 2007, ApJ, 671, 1098
Peng, C. Y., Ho, L. C., Impey, C. D., & Rix, H.-W. 2002, AJ, 124, 266
Schawinski, K., Dowlin, N., Thomas, D., Urry, C. M., & Edmondson, E. 2010a, ApJ, 714, L108
Schawinski, K., Thomas, D., Sarzi, M., Maraston, C., Kaviraj, S., Joo, S.-J., Yi, S. K., & Silk, J. 2007, MNRAS, 382, 1415
Schawinski, K., Virani, S., Simmons, B., Urry, C. M., Treister, E., Kaviraj, S., & Kushkuley, B. 2009, ApJ, 692, L19
Schawinski, K., et al. 2010b, ApJ, 711, 284
Sersic, J. L. (ed.) 1968, Atlas de Galaxias Australes (Cordoba: Observatorio Astronomico)
Simmons, B. D., & Urry, C. M. 2008, ApJ, 683, 644
Springel, V., Di Matteo, T., & Hernquist, L. 2005, MNRAS, 361, 776
Treister, E., Natarajan, P., Sanders, D. B., Urry, C. M., Schawinski, K., & Kartaltepe, J. 2010, Science, 328, 600
Treister, E., Urry, C. M., & Virani, S. 2009a, ApJ, 696, 110
Treister, E., et al. 2009b, ApJ, 706, 535
Trump, J. R., et al. 2009, ApJ, 700, 49
Ueda, Y., Akiyama, M., Ohta, K., & Miyaji, T. 2003, ApJ, 598, 886
Wild, V., Kauffmann, G., Heckman, T., Charlot, S., Lemson, G., Brinchmann, J., Reichard, T., & Pasquali, A. 2007, MNRAS, 381, 543
Windhorst, R. A., et al. 2010, arXiv:1005.2776